The CygnusX Legacy Project
Data Description:

Delivery 1: July 2011

CygnusX team: Joseph L. Hora[1] (PI), Sylvain Bontemps[2], Tom Megeath[3], Nicola Schneider[4] , Frederique Motte[4], Sean Carey[5], Robert Simon[6], Eric Keto[1], Howard Smith[1], Lori Allen[7], Rob Gutermuth[8], Giovanni Fazio[1], Kathleen Kraemer[9], Don Mizuno[10], Stephan Price[9], Joseph Adams[11], Xavier Koenig[12]

[1]Harvard-Smithsonian Center for Astrophysics, [2]Observatoire de Bordeaux, [3]University of Toledo, [4]CEA-Saclay, [5]Spitzer Science Center, [6]Universität zu Köln, [7]NOAO, [8]Smith College, [9]Air Force Research Lab, [10]Boston College, [11]Cornell University, [12]Goddard Space Flight Center

Table of Contents

1. Project Summary

The Cygnus-X project is a Cycle 4 Legacy program (PID 40184) on the Spitzer Space Telescope (Hora et al. 2007). The project is described more fully in Hora et al. (2011, in preparation; also see Kraemer et al. 2010, Beerer et al. 2010). The team maintains a public Cygnus-X project web site at http://www.cfa.harvard.edu/cygnusX/.

The Cygnus-X region is one of the brightest regions of the sky at all wavelengths and one of the richest known regions of star formation of the Galaxy. It contains as many as 800 distinct H II regions, a number of Wolf-Rayet and O3 stars and several OB associations, including Cyg OB2, Cyg OB1, and Cyg OB9. At a distance of ~1.7 kpc (Schneider et al. 2006), Cygnus X is the largest known molecular complex within 2 kpc. With a total mass of ~3×10^6 $M_\odot$, Cygnus-X has three times the combined mass of the molecular clouds within 500 pc of the Sun, in a region 1/5 the diameter. It contains the Cygnus OB2 association, the most massive OB association known near the Sun (Knödlseder 2000, Hanson 2003, Wright & Drake 2010). This massive complex is a unique laboratory for understanding star formation in massive complexes and for studying the formation of stars with masses >1 $M_\odot$. The goals of the Cygnus-X survey are to provide a detailed picture of the processes that govern the evolution of massive star forming complexes, to study star formation in the massive star forming complex environment, and to provide a rich sample of intermediate to high mass protostars spanning the full range of protostellar evolution. The project will also allow us to assess the role of feedback in a massive OB star/molecular cloud complex.

The survey imaged a ~24 square degree region centered near 20:30:25, +40:00 (J2000). The IRAC images had a median coverage of 3x12s high dynamic range (HDR) frames, and the MIPS data were taken in fast scanning mode in the 24 and 70 μm bands. A color mosaic of the survey data in the 3.6, 8.0, and 24 μm bands is shown in Figure 1.

1.1 IRAC observations

Because the region is much larger than what can be accomplished with a single AOR, tiles of ~1.1°×1.1° were planned to cover the survey area. Each tile was composed of a rectangular mapping pattern using a regular grid pattern of 12 columns and 36 rows, with steps of 300 arcsec between columns and 100 arcsec between rows, resulting in a median coverage of 3 frames at each integration time, with some higher overlap regions to ensure that no gaps in coverage exist, and the three observations are at different positions on the array.

In order to maximize the survey area, we designed the AORs for the specific range of dates that the program was scheduled by the SSC. This allowed us to map the largest area possible in the given time, and ensure that there would not be gaps in the survey between the tiles. Unfortunately, not all of the IRAC observations could be scheduled during a single campaign, and in fact the data were obtained in three separate campaigns from 2007 November to 2008 November, as detailed in Table 1 (campaigns IRAC-46, IRAC-54, and IRAC-56). Several AORs in regions containing bright stars had to be scheduled at the end of a campaign to prevent them from affecting other programs. Also, because of the different rotation angles between the AORs in different campaigns, the tiles had to be repositioned, and several small AORs constructed to

fill the regions between the epochs. This led to more AORs than would have been necessary had they been executed back-to-back, but in the end the survey requirements were met by the observations that were performed.

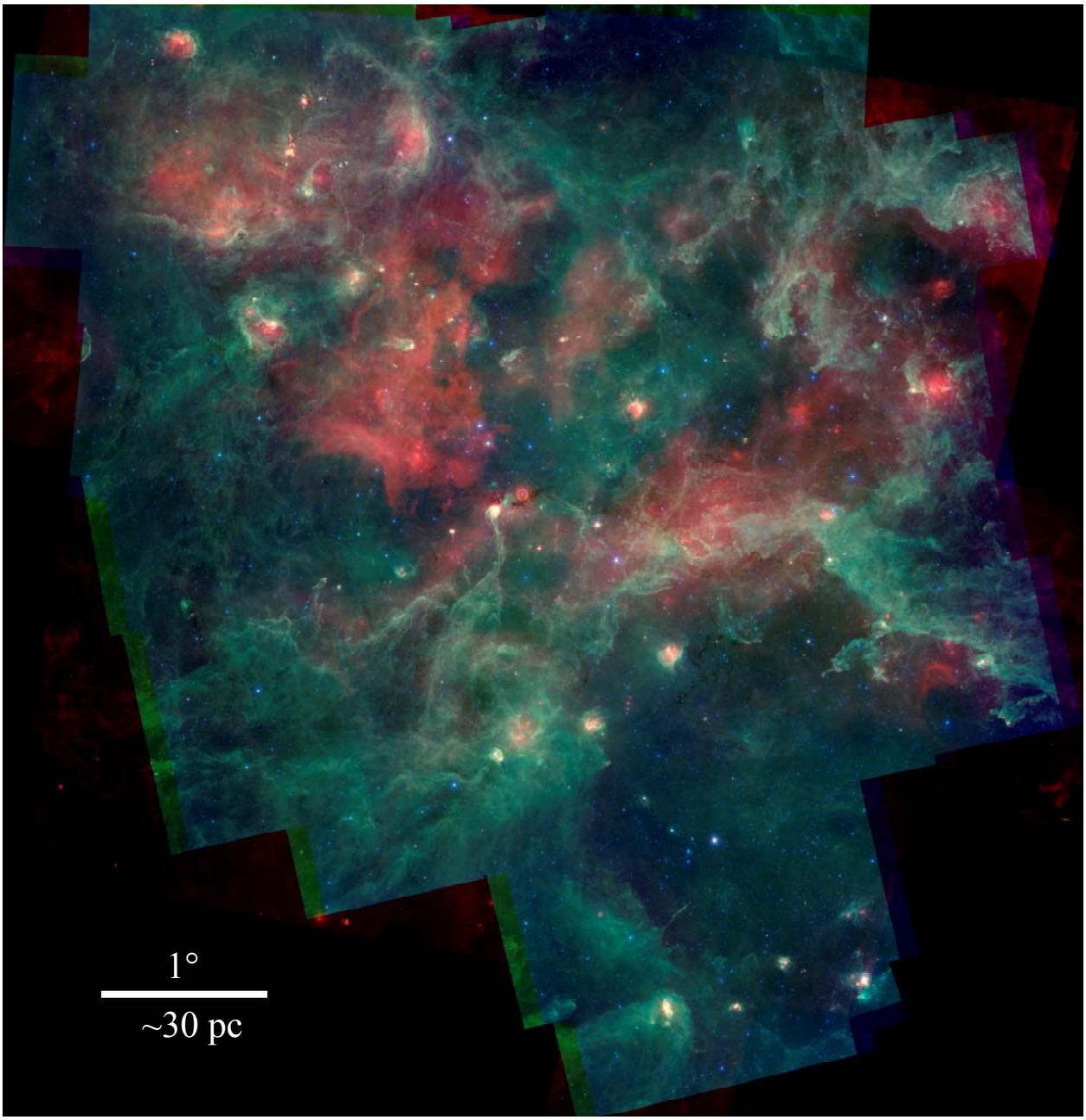

Figure 1. The Cygnus-X Legacy Survey image, courtesy of R. Hurt (Caltech). The MIPS 24 μm image is red, 8.0 μm in green, and 3.6 μm is blue in this mosaic. The vertical size of this image is approximately 6.5°. The 1° scale bar is equivalent to ~30 pc at the adopted distance of 1.7 kpc.

1.2 MIPS observations

We employed a MIPS mapping strategy similar to that used in the MIPSGAL Legacy project (Carey et al. 2009). The area is mapped by narrow fast scan maps using an offset of 14800 arcsec between scan legs. A scan length of 5 degrees was used for most of the AORs. Each position was sampled at least 10 times at 24 μm for a total of 30s on-source integration time. The redundancy

is 5 times in the 70 μm array with this scan pattern, for a 15s on-source time. The survey region was covered with 19 of the 5 degree scans, overlapping slightly between adjacent scans, which covered a roughly square region. Three additional AORs were used to extend the coverage slightly to cover the designated survey region. The total time required for the MIPS observations was 61 hours, and these were completed during a single MIPS campaign (MIPS46) in 2007 November- December. The details are given in Table 1.

1.3 Data reduction

1.3.1 IRAC reduction

All IRAC observations were obtained in HDR mode, whereby two images are taken in succession at 0.4s and 10.4s integration times. We utilized standard Basic Calibrated Data (BCD) version S18.5 products from the Spitzer Science Center's standard data pipeline. The BCD images were first improved with custom treatments for bright source artifacts ("pulldown", "muxbleed", and "banding"; Hora et al. 2004; Pipher et al. 2004). Then all frames were combined into mosaics with WCSmosaic (Gutermuth et al. 2008b) such that rotation, spatial scale distortion, and subpixel offset resampling are all performed in one transformation, to minimize smoothing. IRAC mosaics were constructed at their native pixel scale of 1.2″ per pixel, and angular resolutions range from 2.0″ to 2.5″ full width at half maximum, varying by bandpass. Redundancy-based outlier detection and removal is also performed during mosaic construction, eliminating transient signals such as cosmic ray hits.

Automated source detection and aperture photometry were performed using PhotVis version 1.10 (Gutermuth et al. 2008b). PhotVis utilizes a modified DAOphot (Stetson 1987) source-finding algorithm which calculates local noise across the mosaics and uses this noise map to set a position dependent detection threshold. This technique provides robust source detection in fields with bright, spatially varying nebulosity. Aperture photometry was performed using synthetic apertures of 2.4″ radius, with background annuli of inner and outer radii of 2.4″ and 7.2″, respectively. These aperture and annulus sizes have been adopted as a practical way of adequately sampling the core of the point spread function (PSF) while minimizing contamination from resolved background emission and other nearby sources (Megeath et al. 2004). The PhotVis default S/N cutoff level of 7 was used. Photometric calibration values adopted (Vega-standard magnitudes for 1 DN s^{-1} are identical to those used by Gutermuth et al. (2008b): 19.455, 18.699, 16.498, and 16.892 for 3.6, 4.5, 5.8 and 8.0 μm bands respectively. These values are derived from the calibration effort presented in Reach et al. (2005), and they include standard corrections for the aperture sizes chosen. The calibration uncertainties are approximately 5% across all IRAC bands.

Earlier evaluation of IRAC BCDs revealed that up to 50% of the radial astrometric residuals to 2MASS (Skrutskie et al. 2006) point source catalog positions are caused by simple full field offsets that seem to vary from AOR to AOR. Before building the final mosaics that are sometimes composed of more than one AOR of BCD images, the data from each AOR were separately run through the above mosaicking, point source extraction, and catalog merger processes in order to measure this offset and improve the astrometric calibrations. The median offset applied is ~0.3″. The final spread of radial astrometric residuals relative to 2MASS are typically 160 milli-arcseconds in the 3.6, 4.5, and 5.8 μm channel mosaics, and 180 milli-arcseconds for the 8.0 μm channel mosaic.

Table 1. Cygnus-X Project Observation Summary

AOR ID	Instrument	Date start	R.A.	Declination
22497792	IRAC	2007-11-21	20h42m44.97s	+42d40m30s
22498048	IRAC	2007-11-22	20h37m58.19s	+42d40m30s
22498560	IRAC	2007-11-23	20h28m24.62s	+42d40m30s
22498816	IRAC	2007-11-23	20h23m37.82s	+42d40m30s
22499072	IRAC	2007-11-23	20h46m15.40s	+42d13m30s
22499328	IRAC	2007-11-23	20h42m44.97s	+41d45m54s
22499584	IRAC	2007-11-24	20h37m58.19s	+41d45m54s
22499840	IRAC	2007-11-24	20h33m11.39s	+41d45m54s
22500096	IRAC	2007-11-24	20h28m24.62s	+41d45m54s
22500352	IRAC	2007-11-25	20h23m37.82s	+41d45m54s
22500608	IRAC	2007-11-25	20h19m23.00s	+41d38m00s
22500864	IRAC	2007-11-25	20h42m44.97s	+40d51m18s
24481792	MIPS	2007-11-30	20h44m04.09s	+40d50m43s
24482048	MIPS	2007-11-30	20h45m42.00s	+42d08m00s
22508544	MIPS	2007-12-01	20h42m40.29s	+40d47m54s
22508800	MIPS	2007-12-01	20h41m16.49s	+40d45m05s
22509056	MIPS	2007-12-01	20h39m52.69s	+40d42m17s
22509312	MIPS	2007-12-01	20h38m28.89s	+40d39m28s
22509568	MIPS	2007-12-01	20h37m05.09s	+40d36m39s
22509824	MIPS	2007-12-02	20h35m41.30s	+40d33m50s
22510080	MIPS	2007-12-02	20h34m17.50s	+40d31m01s
22510336	MIPS	2007-12-02	20h32m53.69s	+40d28m13s
22510592	MIPS	2007-12-03	20h31m29.90s	+40d25m24s
22510848	MIPS	2007-12-03	20h30m06.11s	+40d22m35s
22511104	MIPS	2007-12-03	20h28m42.31s	+40d19m46s
22511360	MIPS	2007-12-03	20h27m18.51s	+40d16m58s
22511616	MIPS	2007-12-03	20h25m54.71s	+40d14m09s
22511872	MIPS	2007-12-04	20h24m30.92s	+40d11m20s
22512128	MIPS	2007-12-04	20h23m07.11s	+40d08m31s
22512384	MIPS	2007-12-04	20h21m43.31s	+40d05m42s
22512640	MIPS	2007-12-04	20h20m19.52s	+40d02m54s
22512896	MIPS	2007-12-04	20h18m55.72s	+40d00m05s
22513408	MIPS	2007-12-05	20h16m16.12s	+39d24m00s
23710976	MIPS	2007-12-05	20h27m30.00s	+37d23m00s
27108352	IRAC	2008-08-18	20h29m43.59s	+37d51m59s
27108608	IRAC	2008-08-18	20h26m04.80s	+37d14m56s
27107072	IRAC	2008-08-19	20h26m42.51s	+38d57m05s
27107328	IRAC	2008-08-19	20h25m28.94s	+37d56m23s
27109632	IRAC	2008-08-19	20h17m54.24s	+39d22m51s
27110400	IRAC	2008-08-19	20h22m12.11s	+39d10m18s
27110912	IRAC	2008-08-19	20h22m13.32s	+38d07m44s
27107840	IRAC	2008-08-20	20h32m20.32s	+39d36m51s
27108096	IRAC	2008-08-20	20h31m12.91s	+38d43m53s
27109376	IRAC	2008-08-20	20h19m11.76s	+40d15m46s
27111424	IRAC	2008-08-20	20h36m50.73s	+39d23m39s
27111680	IRAC	2008-08-20	20h35m43.32s	+38d30m40s
27112448	IRAC	2008-08-20	20h40m32.50s	+39d00m11s
27105792	IRAC	2008-08-21	20h18m00.00s	+42d00m00s
27106304	IRAC	2008-08-21	20h20m00.72s	+41d24m25s
27106560	IRAC	2008-08-21	20h28m57.35s	+40d43m02s
27108864	IRAC	2008-08-21	20h45m34.73s	+43d32m27s
27109120	IRAC	2008-08-21	20h19m54.84s	+40d59m47s
27109888	IRAC	2008-08-21	20h24m26.94s	+40d56m15s
27107584	IRAC	2008-08-22	20h33m27.75s	+40d29m50s
27111168	IRAC	2008-08-22	20h37m58.15s	+40d16m37s
27110656	IRAC	2008-08-23	20h33m17.52s	+42d41m49s
27106048	IRAC	2008-08-23	20h38m24.00s	+41d03m43s
27111936	IRAC	2008-08-23	20h28m45.58s	+41d19m40s
27112192	IRAC	2008-08-23	20h42m14.96s	+40d04m57s
27112704	IRAC	2008-08-23	20h33m12.00s	+41d15m03s
27106816	IRAC	2008-08-24	20h27m49.93s	+39d50m04s
27110144	IRAC	2008-08-24	20h23m19.53s	+40d03m16s
27989760	IRAC	2008-11-13	20h21m48.80s	+37d29m54s
27990016	IRAC	2008-11-13	20h25m58.80s	+38d21m50s

1.3.2 MIPS reduction

The reduction of the MIPS data followed techniques developed for the MIPSGAL data (Mizuno et al. 2008). Substantial processing beyond the Spitzer-provided basic calibrated data (BCDs) was necessary for the MIPSGAL data. For both the 24 and 70 μm data, we start with the raw image files and the calibration products provided by the Spitzer Science Center. The MIPSGAL team developed and used a BCD pipeline parallel to the Spitzer version. This alternate pipeline was necessary because the version (S14) of the Spitzer pipeline available when the MIPSGAL data were being processed contained errors in the linearity correction and pixel replacement modules. Our pipeline produces a product equivalent to the Spitzer-provided BCDs. We use the same flux conversion factor (0.0447 MJy sr^{-1} DN^{-1} s) as the Spitzer pipeline. Significant artifacts were produced at 24 μm by the many bright sources imaged during each scan of the Galactic plane. In addition, the bright background level of the Galactic plane necessitated mitigation algorithms other than those recommended in the MIPS Data Handbook. The 24 μm BCDs were post-processed to remove and/or mitigate data artifacts not corrected in the basic pipeline. Details of the post-processing and BCD pipeline modifications are described in Mizuno et al. (2008).

The point sources were extracted from the 24 μm data with Cluster Grinder and PhotVis, as was described above for the IRAC data. See Gutermuth et al. (2009) for more details of the process. We used a synthetic aperture radius of 7.6″ and background annulus inner and outer radii of 7.6″ and 17.8″ for the 24 μm data to match the core of the PSF and minimize the effects of contamination.

2. Point Source Catalog

2.1 Astrometry and catalog matching

Source list matching is performed in stages to minimize mismatches. First, the IRAC data of the four bandpasses were merged, using a maximum radial matching tolerance of 1″. Then the mean positions of each merged entry from that catalog were merged with the 2MASS point source catalog, again using a maximum 1″ radial matching tolerance. Finally, the MIPS 24 μm source list is matched to the mean positions of each entry in this secondary catalog, using a 1.3″ radial matching tolerance to account for the lower resolution and less precise astrometry of these longer wavelength data. Note that the latter matching tolerance is significantly smaller than the 3″ tolerance used by Gutermuth et al. (2008b). This is largely a product of the astrometric recalibration efforts applied to the IRAC and MIPS data, and results in more robust matching of the lower resolution MIPS data, with considerably reduced mismatching rates.

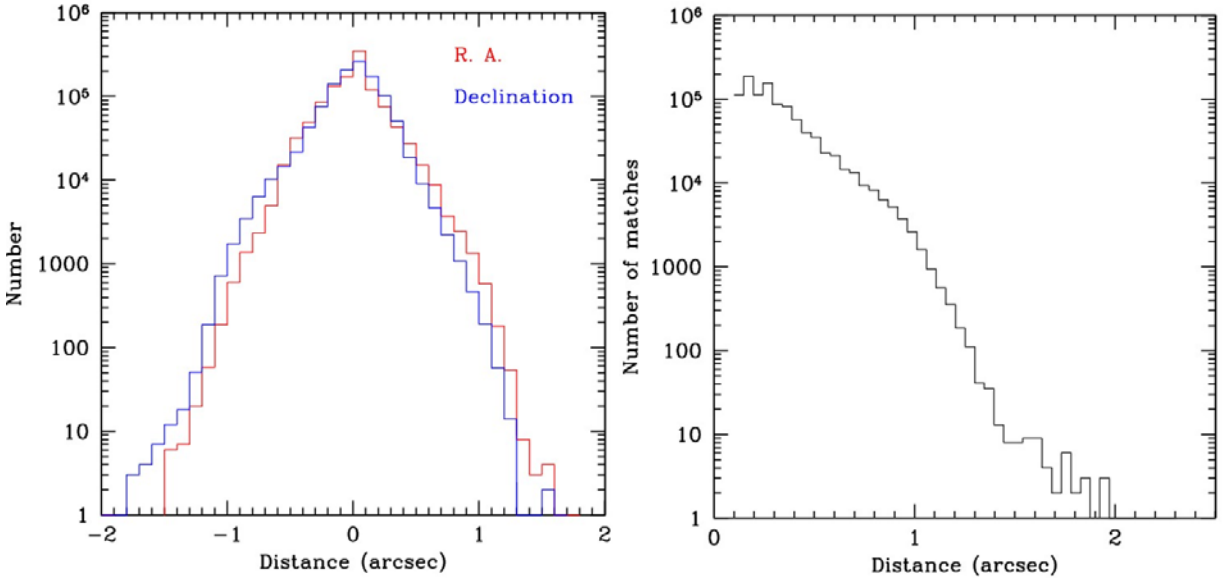

Figure 2. The offsets between the 2MASS and IRAC source positions. For all objects detected in 2MASS and at least one IRAC band, the distance between the positions is shown. The shortest wavelength IRAC channel where the object was detected is used for the IRAC position.

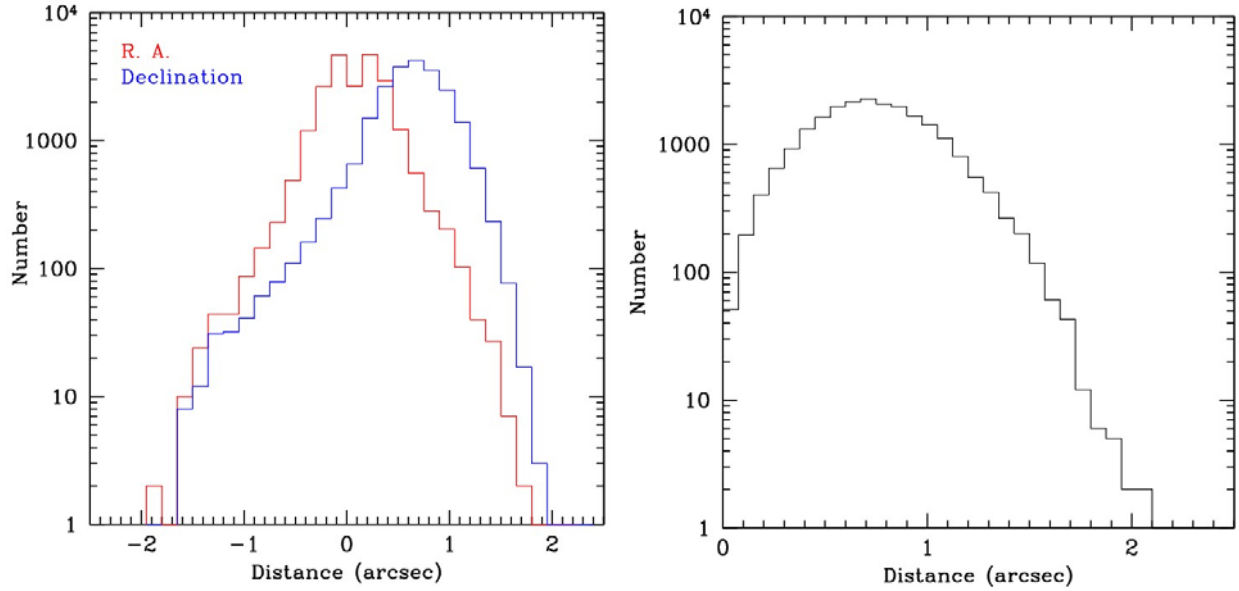

Figure 3. The offsets between the 2MASS and MIPS source positions is shown. There is an approximately 0.7 arcsec offset in the median of the MIPS positions, mainly in the Declination direction.

2.2 Source Lists in the Delivery

Two data products were then selected from the merged full list, the Archive and the Catalog, which are described below. The Catalog has more stringent constraints on S/N and detections in multiple bands, so in principle it is more reliable than the Archive. However, as is apparent from the figures below, the lists differ mostly in the sources included at the faint end, including more sources that satisfy the S/N criterion in both IRAC 3.6 and 4.5 μm bands. A detailed comparison

between the Archive sources and the mosaics indicates that most of the sources are likely real, but a conservative estimate of the S/N has pushed them slightly outside of the requirement for inclusion in the Catalog.

2.2.1 Source Archive

The source archive is the more inclusive of the two lists, and therefore possibly less reliable. For a source to be included in the archive, it must satisfy one of the following two conditions:

1. The source must be detected in at least 2 bands (in the IRAC bands or 2MASS), but not only in IRAC bands 3 and 4.
2. The source must be detected with a S/N>5 in either the IRAC 3.6 or 4.5 μm bands.
3. The source is detected in both IRAC 8.0 μm and MIPS 24 μm bands.

We determined from examining the images and raw source list that an object that appeared in only bands 3 and 4 together was almost without exception a result of the bright source artifact that is a feature of these two channels.

2.2.2 Source Catalog

The source Catalog is more restrictive of the two lists, and so is therefore more reliable than the Archive, but this also means that there are valid sources that are not contained in the Catalog due to the selection criteria. For a source to be included in the catalog, it must satisfy one of the following conditions:

1. The source must be detected in 2 Spitzer bands, at least one of them with S/N>5 (but not in only channel 3 and 4).
2. The source must be detected in 2 IRAC bands and in one of the 2MASS bands.
3. The source must be detected in one of the IRAC bands 1 or 2 with a SN>5, and detected by 2MASS.
4. The source must be detected with a S/N>5 in both IRAC 8.0 μm and MIPS 24 μm bands.

A summary of the number of sources in the Catalog and Archive are given in Table 2.

Table 2. Source Counts in the Catalog and Archive

Cygnus-X List	Total sources	3.6 μm Sources	4.5 μm Sources	5.8 μm Sources	8.0 μm Sources	24 μm Sources
Catalog	2,804,385	2,756,953	2,762,950	822,744	462,065	26,467
Archive	3,521,905	3,263,725	3,036,121	823,344	463,305	27,498

2.3 Source Counts and Completeness

2.3.1 Source Counts

The source count histograms for the Catalog and Archive are shown in Figure 4 to Figure 8. The primary difference between the lists is apparent in the 3.6 and 4.5 μm band, where the Archive contains more objects with lower S/N at the faint end of the distribution.

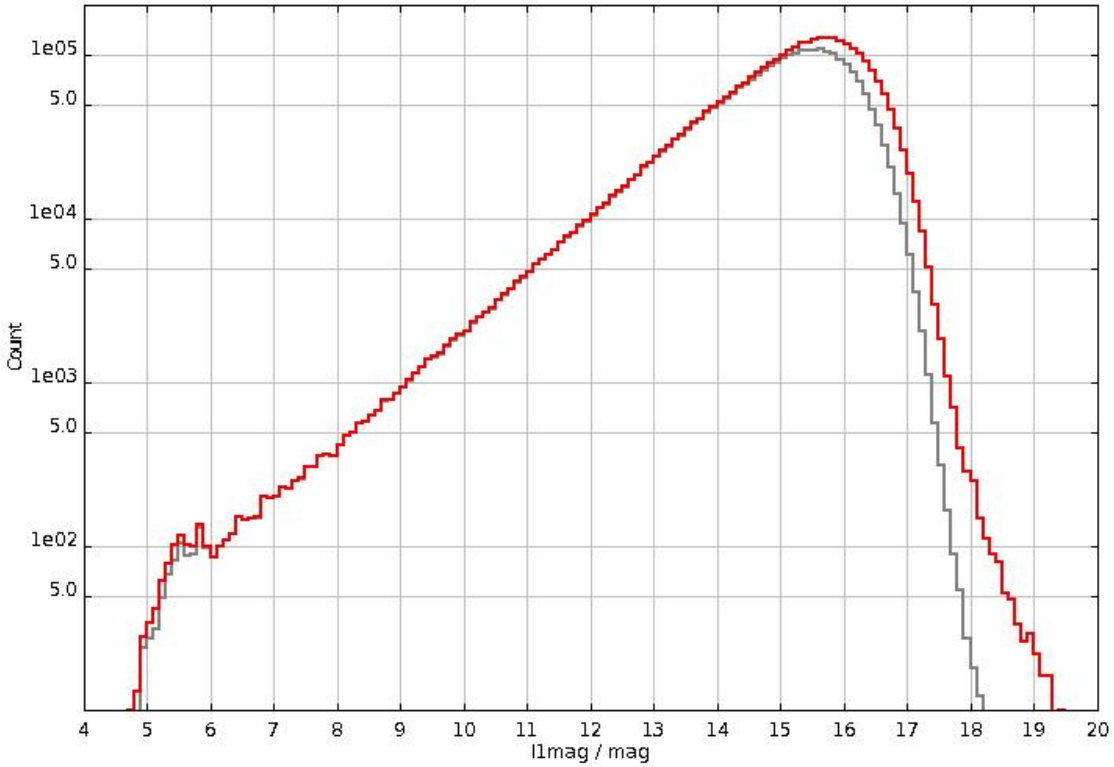

Figure 4. Source counts histograms for IRAC 3.6 μm band. The grey histogram is for the Catalog, and the red histogram is the Archive.

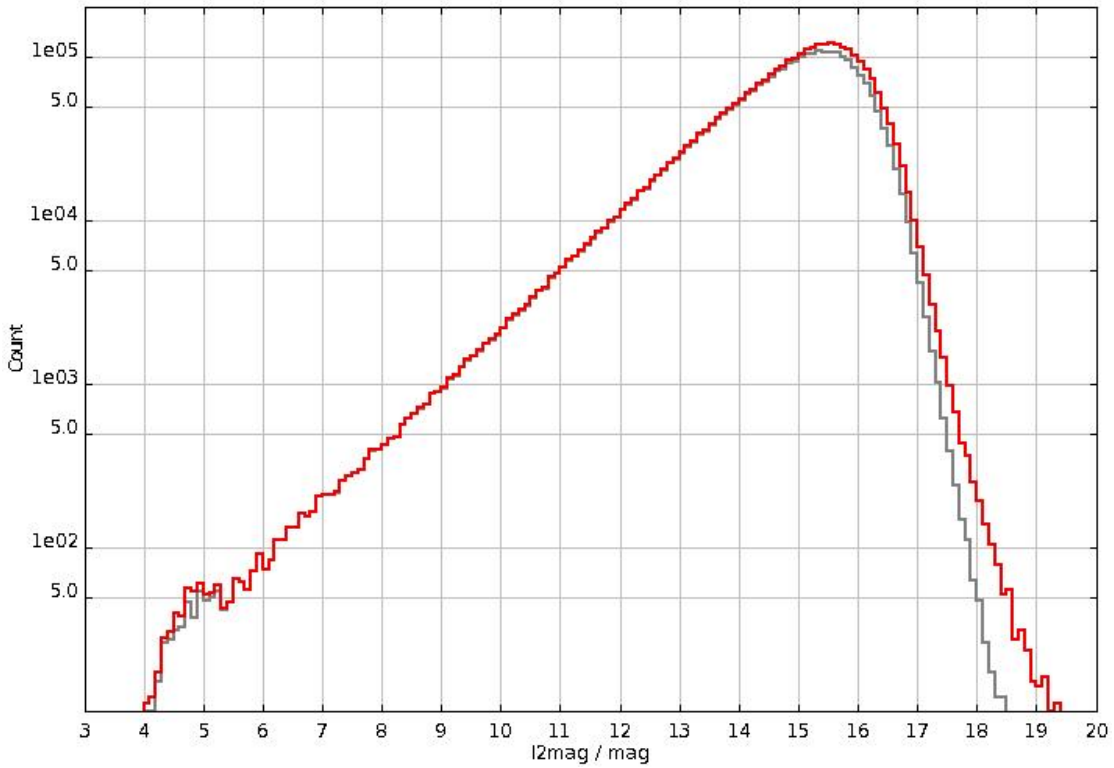

Figure 5. Source counts histograms for IRAC 4.5 μm band. The grey histogram is for the Catalog, and the red histogram is the Archive.

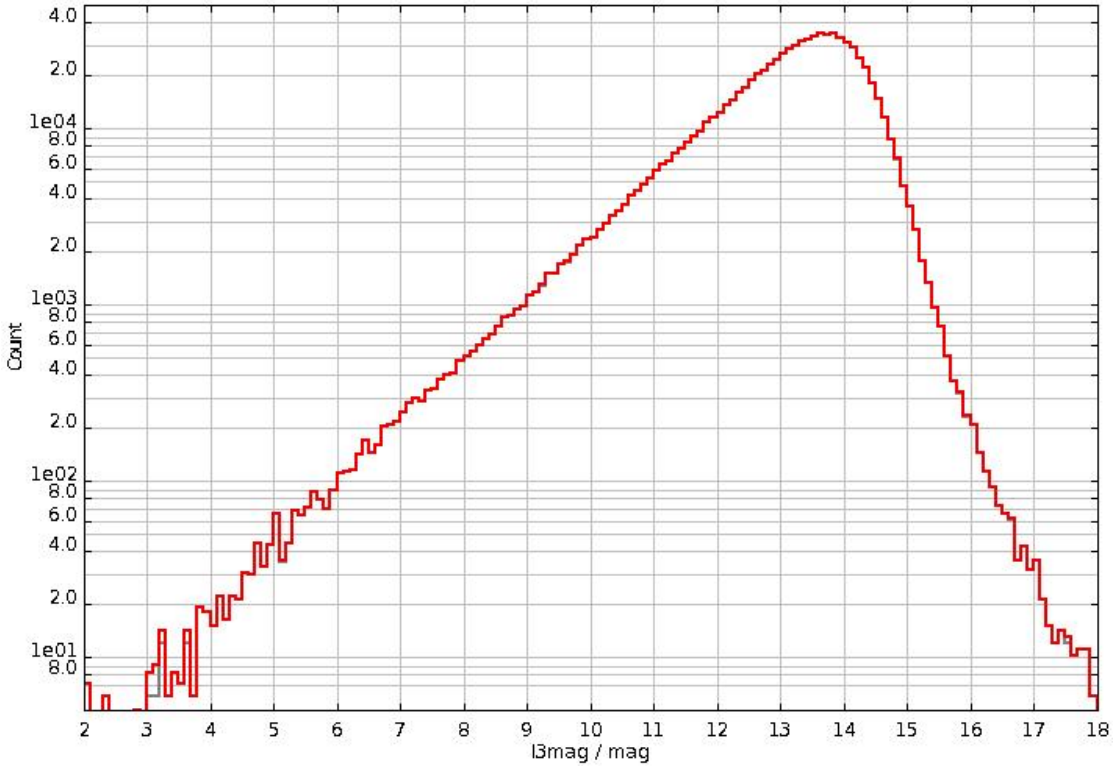

Figure 6. Source counts histograms for IRAC 5.8 μm band. The grey histogram is for the Catalog, and the red histogram is the Archive

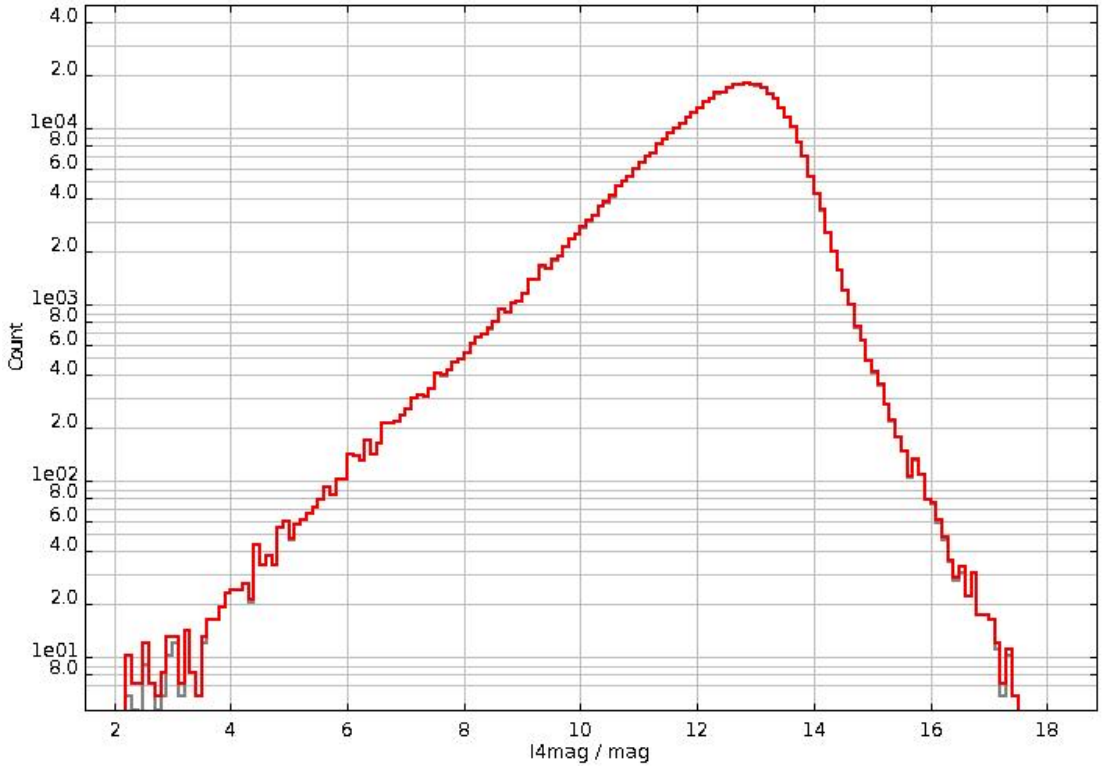

Figure 7. Source counts histograms for IRAC 8.0 μm band. The grey histogram is for the Catalog, and the red histogram is the Archive.

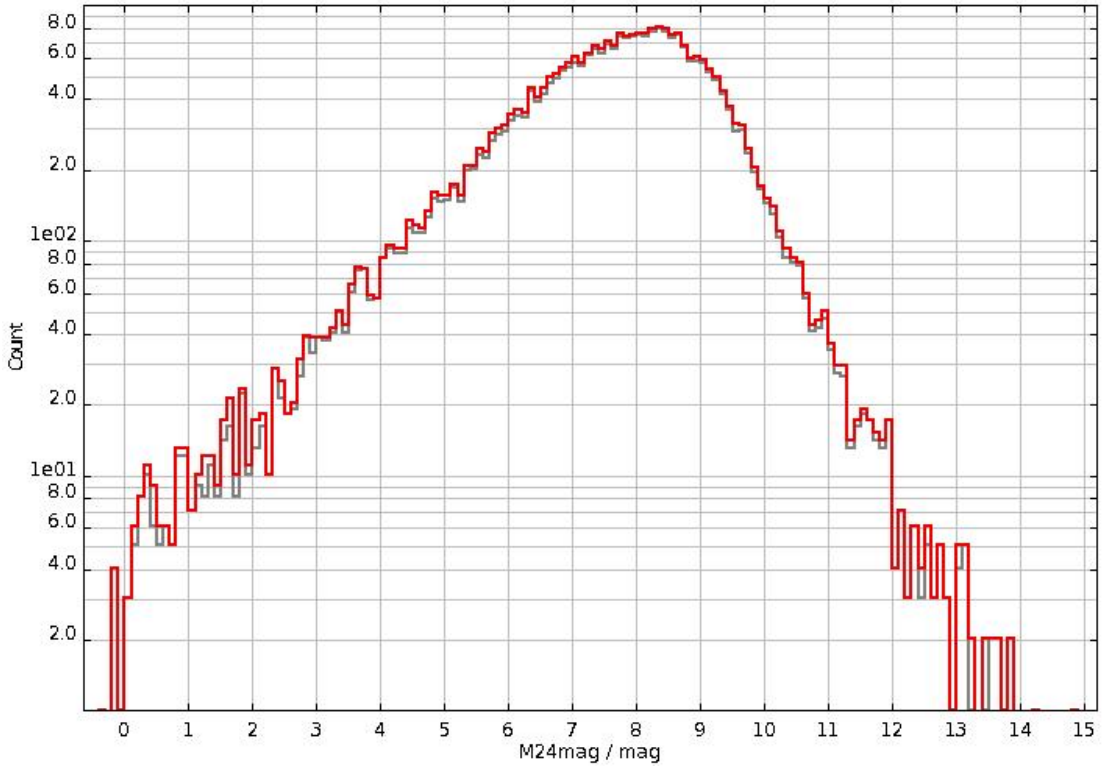

Figure 8. Source counts for MIPS 24 μm sources. The grey histogram is for the Catalog, and the red histogram is the Archive

2.3.2 Completeness Estimate

The completeness of the IRAC data was estimated by adding artificial sources of various magnitudes to a sample region of the Cygnus survey image, and then performing the source finding analysis and photometry extraction on the simulated sources in the same manner as the real catalog was produced in order to assess its ability to extract the photometry accurately. The sample region (centered on 20:27:07, +40:00:00, 1.8°×1.8° in size) was chosen to be typical of the mix of sources in the survey, including regions of bright extended background emission, dark clouds, dense clusters, and relatively uncrowded regions. The results of the completeness estimate are shown in Figure 9. For each of the IRAC bands, the percent of the input sources extracted are shown as a function of the source magnitude. The source had to be within 0.5″ of the position of the artificial source to be considered a match. The 90% completeness levels for IRAC channels 1, 2, 3, and 4 are 14.98, 14.87, 13.82, and 12.60 magnitude, respectively. The standard deviation of the magnitude errors for sources at the 90% completeness limit was ~0.3 mag.

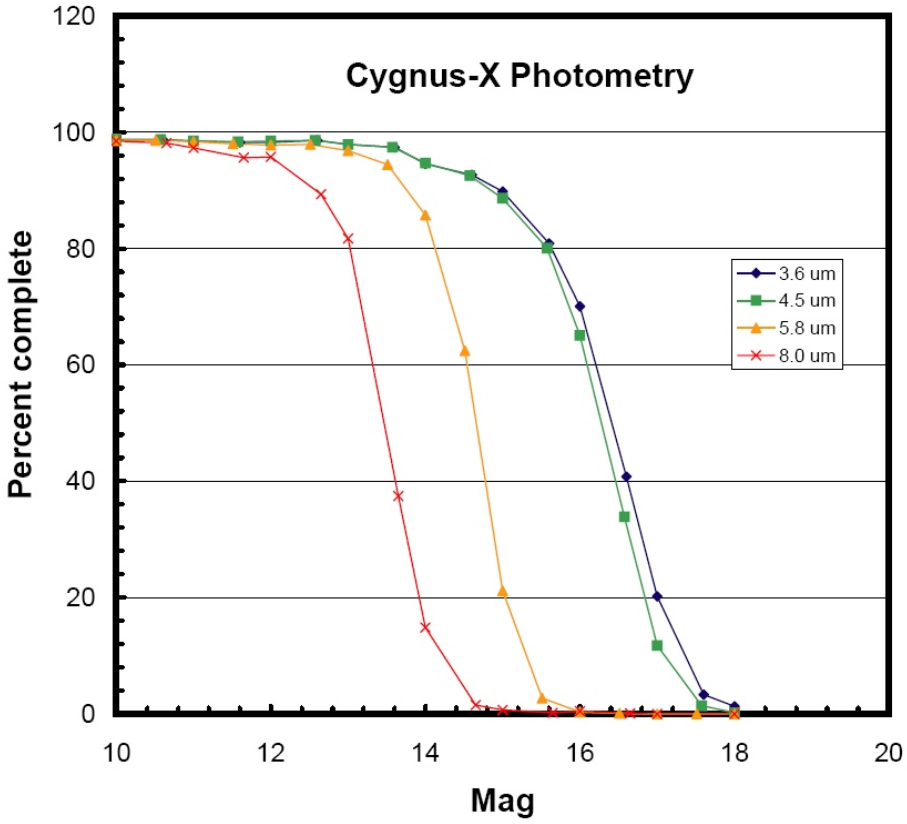

Figure 9. An estimate of the completeness of the IRAC data as a function of magnitude for the Cygnus survey.

2.4 Photometric Errors

The error estimate included in the catalog is determined by the PhotVis algorithm when it performs the source photometry. We have RSS'd a noise floor of 0.015 mag to all of the values, which has been determined from other observations to be the repeatability of IRAC measurements in star formation regions with this depth of coverage (e.g. Morales-Calderón et al. 2011). Plots of the magnitude error as a function of magnitude for each of the bands in the Catalog and Archive are shown in Figure 10 to Figure 15.

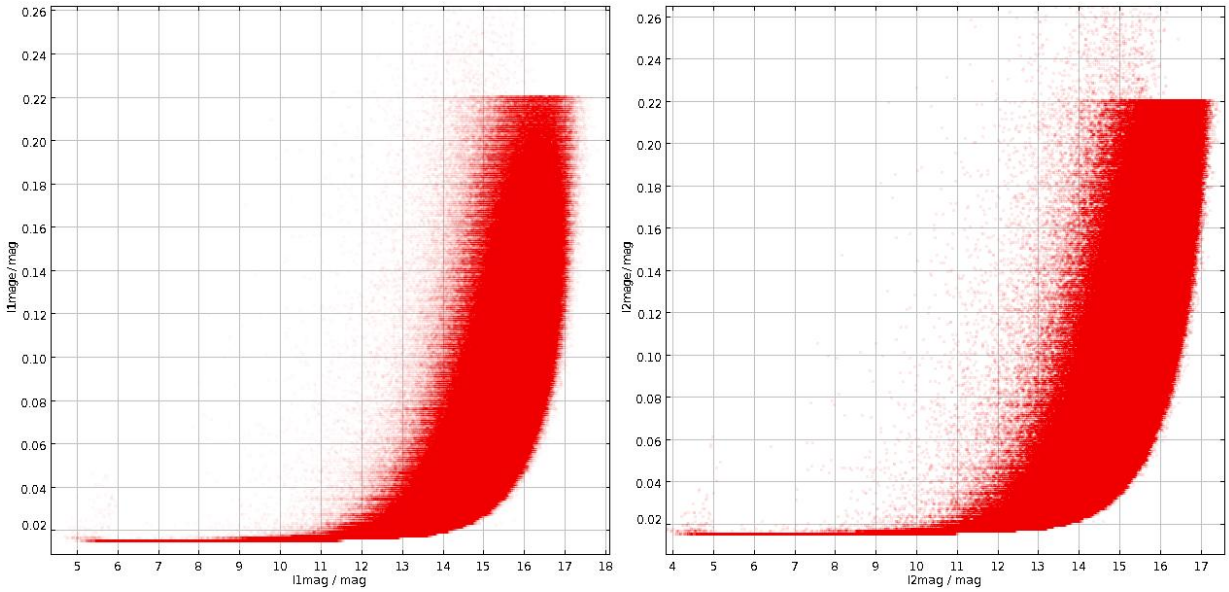

Figure 10. The uncertainty in magnitudes versus magnitude for the IRAC 3.6 (left) and 4.5 μm (right) catalog. Sources above 0.3 uncertainty are not plotted unless they have a detection with an error below 0.22 in another IRAC channel.

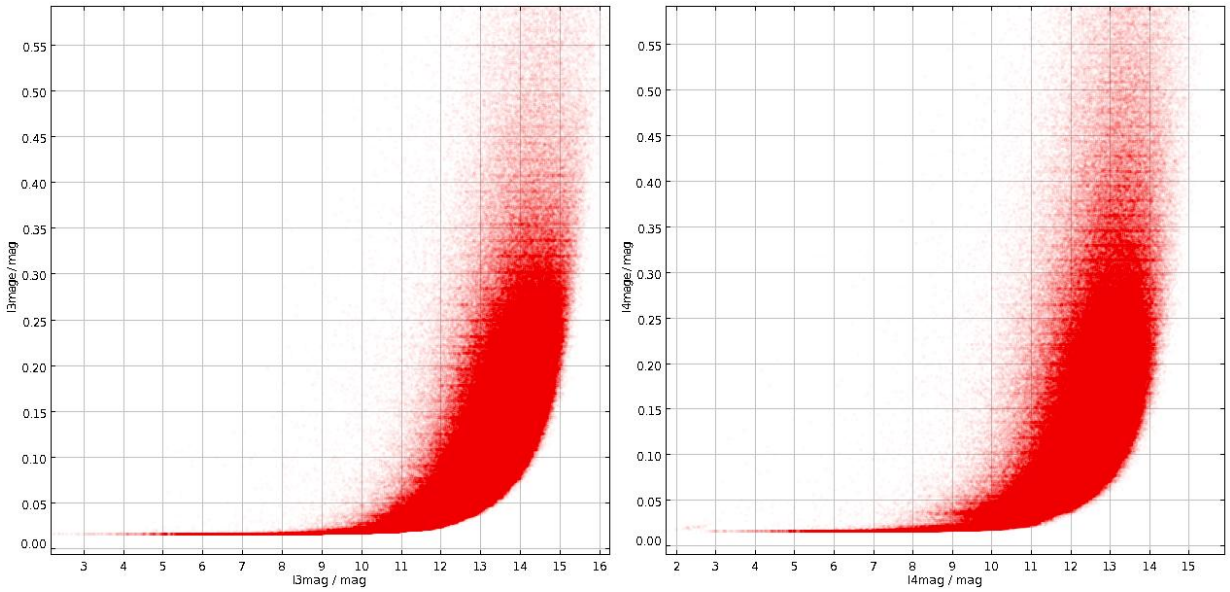

Figure 11. The uncertainty in magnitudes versus magnitude for the IRAC 5.8 (left) and 8.0 μm (right) catalog. Sources above 0.3 uncertainty are not plotted unless they have a detection with an error below 0.22 in another IRAC channel.

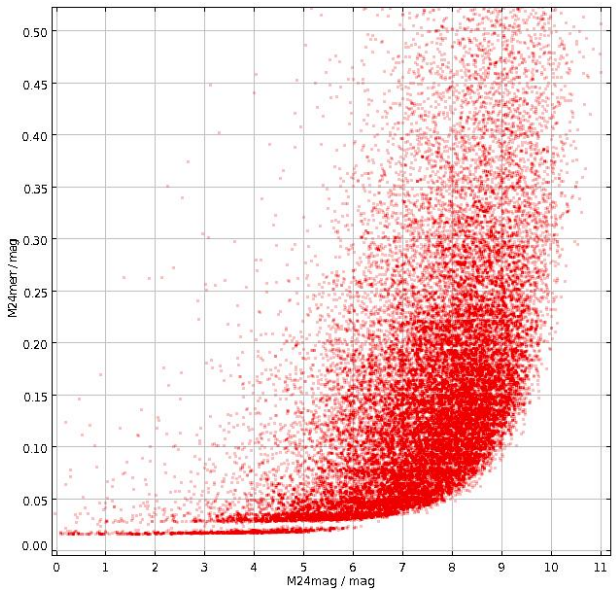

Figure 12. The uncertainty in magnitudes versus magnitude for the MIPS 24 μm data in the catalog.

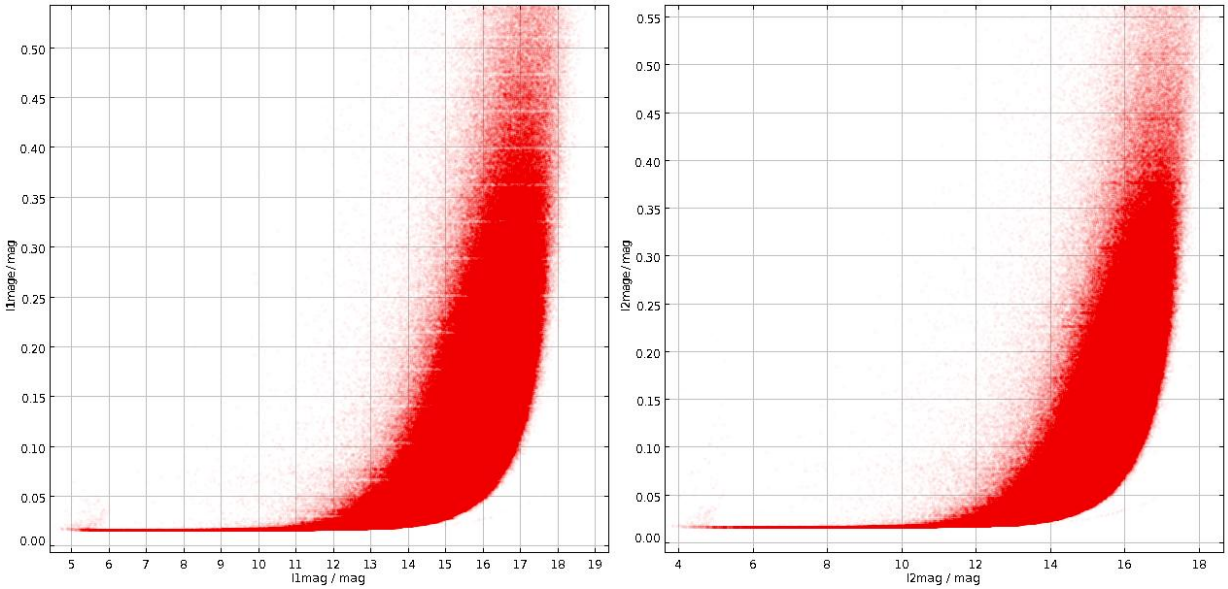

Figure 13. The uncertainty in magnitudes versus magnitude for the IRAC 3.6 (left) and 4.5 μm (right) archive.

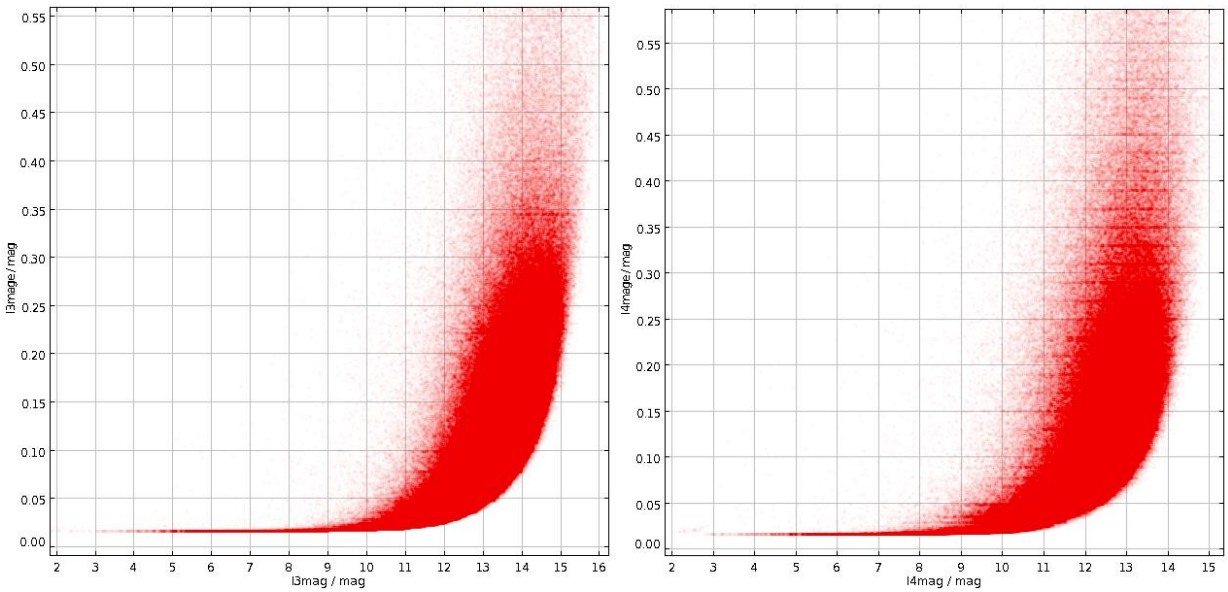

Figure 14. The uncertainty in magnitudes versus magnitude for the IRAC 5.8 (left) and 8.0 µm (right) archive.

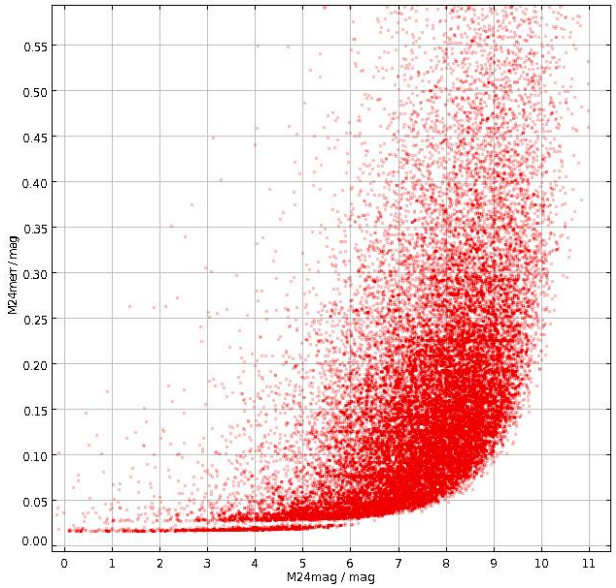

Figure 15. The uncertainty in magnitudes versus magnitude for the MIPS 24 µm data in the archive.

3. Cygnus-X Mosaics

The sections below describe two types of mosaics that are part of the data release. The "Photometry Mosaics" in Section 3.1 were the images used to perform the photometry that is in the Source Catalog and Archive datasets described in Section 2. These mosaics were constructed using one or two AORs each, so are mostly regions of ~1 square degree. This is therefore the set of images to use if one is interested in reproducing the photometry, or performing an enhanced extraction of some region in the survey field.

Section 3.2 describes the "Full Field Mosaics" where we removed residual instrumental background patterns and used background-matching software to construct an image of the full field that was as free as possible of gradients or background mismatches between the individual BCDs which were taken at different times and orientations. These are the mosaics to use if one is interested in examining the extended emission that can stretch across many individual BCDs, or in displaying large regions of the survey field without background artifacts. The full-field mosaic has also been broken up into smaller tiles for ease of use, since the full-resolution mosaics are large in size (~25,000 pixels on a side, ~2.6 GB for each of the IRAC bands).

3.1 IRAC Photometry Mosaics

Because of the number of AORs and the total size of the dataset, the initial mosaicing/photometry step was run on single or small groups of AORs, and the catalog was produced from merging the photometry for each of these individual reductions. This first set of images are the "tiles" from which this photometry was based, and are the direct output of the Cluster Grinder software. We will refer to these mosaics as the "photometry mosaics". These mosaics are included in the release for reference but were not used further in making the full field mosaics described in Section 3.2.

The data were processed mostly using a single AOR per mosaic tile, except for a few small AORs that were combined with adjacent AORs. See the list in the table below for a mapping of each AOR to image tile.

The photometry mosaic files in this delivery have names of the form IX_tileNNNN_mos.fits or IX_tileNNNN_msk.fits, where X is the IRAC channel number (1, 2, 3, or 4 for the 3.6, 4.5, 5.8 and 8 micron channels, respectively), NNNN is the 4-digit tile label (see table Table 3) and the *mos.fits files being the flux image and the *msk.fits file is an image that shows the depth of coverage at each point. The *msk.fits file shows the overlaps between frames, and also where pixels have been rejected due to being bad pixels in the arrays, or having cosmic rays, saturation, or other effects that could cause a pixel to be rejected.

Table 3. Association of AOR number to Photometry Tile name

AORID	Date of Obs	Approximate R.A.	(J2000.0) Decl.	Image Label
22497792	2007-11-21	20h42m44.97s	+42d40m30s	tile7792
22498048	2007-11-22	20h37m58.19s	+42d40m30s	tile8048
22498560	2007-11-23	20h28m24.62s	+42d40m30s	tile8560
22498816	2007-11-23	20h23m37.82s	+42d40m30s	tile8816
22499072	2007-11-23	20h46m15.40s	+42d13m30s	tile9072
22499328	2007-11-23	20h42m44.97s	+41d45m54s	tile9328
22499584	2007-11-24	20h37m58.19s	+41d45m54s	tile9584
22499840	2007-11-24	20h33m11.39s	+41d45m54s	tile9840
22500096	2007-11-24	20h28m24.62s	+41d45m54s	tile0096
22500352	2007-11-25	20h23m37.82s	+41d45m54s	tile0352
22500608	2007-11-25	20h19m23.00s	+41d38m00s	tile0608
22500864	2007-11-25	20h42m44.97s	+40d51m18s	tile0864
27108352	2008-08-18	20h29m43.59s	+37d51m59s	tile8352
27108608	2008-08-18	20h26m04.80s	+37d14m56s	tile8608
27107072	2008-08-19	20h26m42.51s	+38d57m05s	tile7072
27107328	2008-08-19	20h25m28.94s	+37d56m23s	tile0912
27109632	2008-08-19	20h17m54.24s	+39d22m51s	tile9632
27110400	2008-08-19	20h22m12.11s	+39d10m18s	tile0400
27110912	2008-08-19	20h22m13.32s	+38d07m44s	tile0912
27107840	2008-08-20	20h32m20.32s	+39d36m51s	tile7840
27108096	2008-08-20	20h31m12.91s	+38d43m53s	tile8096
27109376	2008-08-20	20h19m11.76s	+40d15m46s	tile9376
27111424	2008-08-20	20h36m50.73s	+39d23m39s	tile1424
27111680	2008-08-20	20h35m43.32s	+38d30m40s	tile1680
27112448	2008-08-20	20h40m32.50s	+39d00m11s	tile2448
27105792	2008-08-21	20h18m00.00s	+42d00m00s	tile5792
27106304	2008-08-21	20h20m00.72s	+41d24m25s	tile6304
27106560	2008-08-21	20h28m57.35s	+40d43m02s	tile1936
27108864	2008-08-21	20h45m34.73s	+43d32m27s	tile8864
27109120	2008-08-21	20h19m54.84s	+40d59m47s	tile9120
27109888	2008-08-21	20h24m26.94s	+40d56m15s	tile9888
27107584	2008-08-22	20h33m27.75s	+40d29m50s	tile7584
27111168	2008-08-22	20h37m58.15s	+40d16m37s	tile6048
27110656	2008-08-23	20h33m17.52s	+42d41m49s	tile0656
27106048	2008-08-23	20h38m24.00s	+41d03m43s	tile6048
27111936	2008-08-23	20h28m45.58s	+41d19m40s	tile1936
27112192	2008-08-23	20h42m14.96s	+40d04m57s	tile2192
27112704	2008-08-23	20h33m12.00s	+41d15m03s	tile7584
27106816	2008-08-24	20h27m49.93s	+39d50m04s	tile6816
27110144	2008-08-24	20h23m19.53s	+40d03m16s	tile0144
27989760	2008-11-13	20h21m48.80s	+37d29m54s	tile9760
27990016	2008-11-13	20h25m58.80s	+38d21m50s	tile0016

3.2 Full-Field Mosaics

3.2.1 IRAC Data Processing

The S18.5 BCDs that were used in this delivery had residual background gradients that were different in each AOR, due to imperfect dark frame subtraction and/or zodiacal background emission differences. These gradients result in background mismatches when the individual AOR mosaics are assembled into an image of the entire Cygnus-X survey area. In order to produce images free of the more serious background artifacts, the "afrl_bcd_overlap" routine (Mizuno et al. 2008) was used to normalize the backgrounds and remove gradients at the BCD level before mosaicing them into the final image. The absolute background levels of the IRAC images are not known, due to the way that the Spitzer data are taken without a zero level reference. The afrl_bcd_overlap method further adjusts the background levels of the images to match levels between overlapping image regions. The background matching will therefore remove any gradients that change from AOR to AOR, such as array artifacts or zodiacal background emission flux or gradients, but it will not produce a reliable measurement of the absolute background or flux at any location.

The Cluster Grinder software produces a set of BCD images with the artifacts such as column pulldown, muxbleed, and banding effects removed to the best of its ability. These images were used as input to the background-matching process. Once the background matching step was completed, the images were then mosaiced with IRACproc (Schuster et al. 2006) which uses a version of the mopex mosaicing software (Makovoz et al. 2005) developed at the SSC. Mosaics were constructed separately for the 12 sec and 0.6 sec frames. The final mosaics in this delivery combined the two sets, using primarily the 12 sec mosaics except where they were non-linear or saturated due to bright sources; in those pixel locations, the 0.6 sec mosaics were used to fill in the image. There are some sources that saturated the images even in the 0.6 sec frames. These locations are typically visible in the final mosaics where the core of a bright source is lower than the surrounding pixels.

3.2.2 Full survey images

The highest resolution images can be difficult to work with because of the memory requirements imposed by the large image sizes. Therefore, for the user's convenience, we have produced several versions of the full survey mosaic images, which are derived from the highest resolution mosaics in each band. The following mosaics of the Cygnus-X Survey data are included in this Release 1.0:

<u>Mosaics at a resolution of 2.4 arcsec/pixel:</u>
IRAC Channel 1 (3.6 μm): I1_cygnus_2.4.fits
IRAC Channel 2 (4.5 μm): I2_cygnus_2.4.fits
IRAC Channel 3 (5.8 μm): I3_cygnus_2.4.fits
IRAC Channel 4 (8.0 μm): I4_cygnus_2.4.fits
MIPS Channel 1 (24 μm): M1_cygnus_2.4.fits

<u>MIPS mosaics at a resolution of 1.2 arcsec/pixel:</u>
MIPS Channel 1 (24 um): M1_cygnus_1.2.fits

Mosaics at a resolution of 0.8626716 arcsec/pixel:
IRAC Channel 1 (3.6 μm): I1_cygnus_0.8.fits
IRAC Channel 2 (4.5 μm): I2_cygnus_0.8.fits
IRAC Channel 3 (5.8 μm): I3_cygnus_0.8.fits
IRAC Channel 4 (8.0 μm): I4_cygnus_0.8.fits

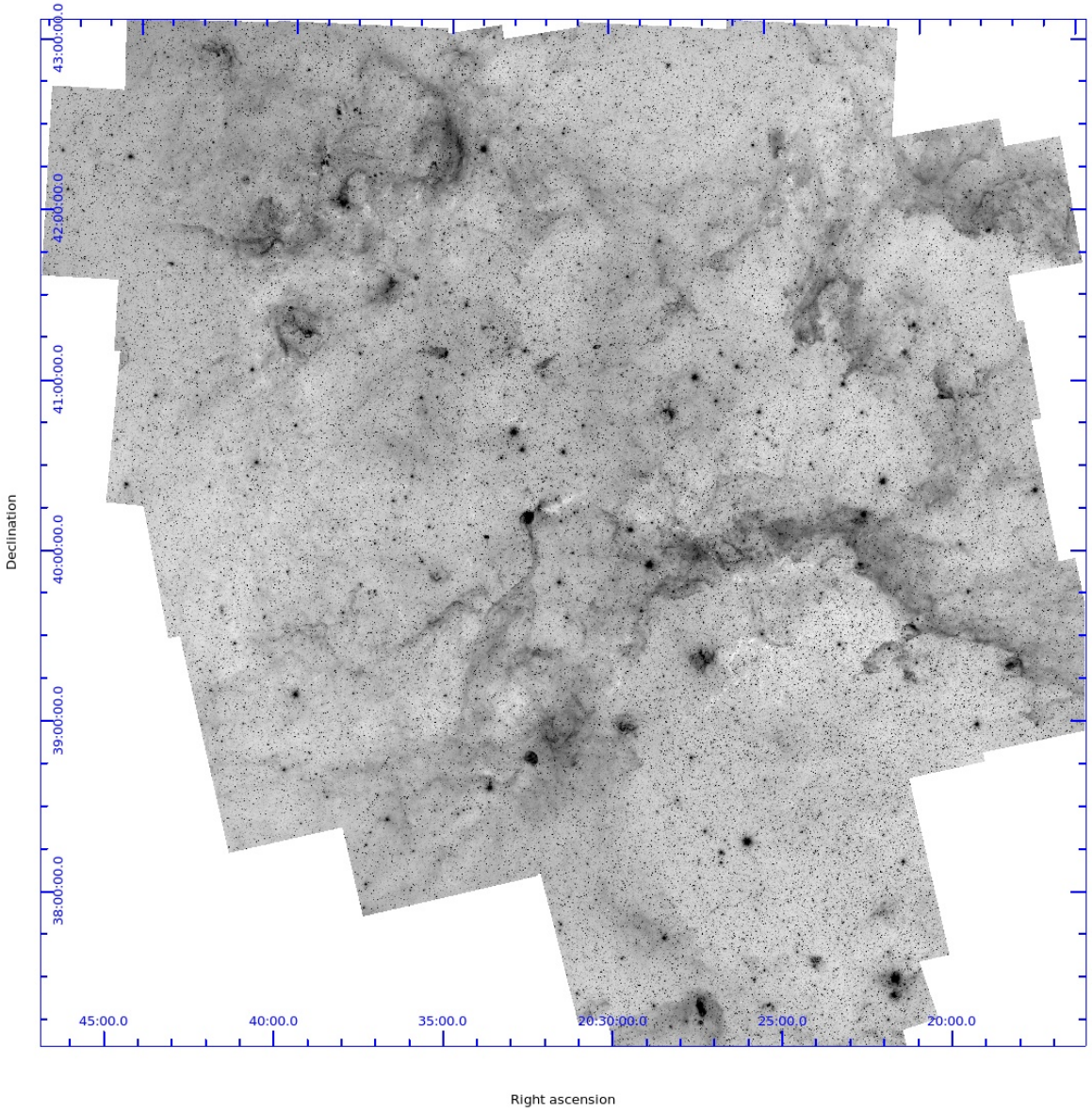

Figure 16. IRAC 3.6 μm full-field mosaic.

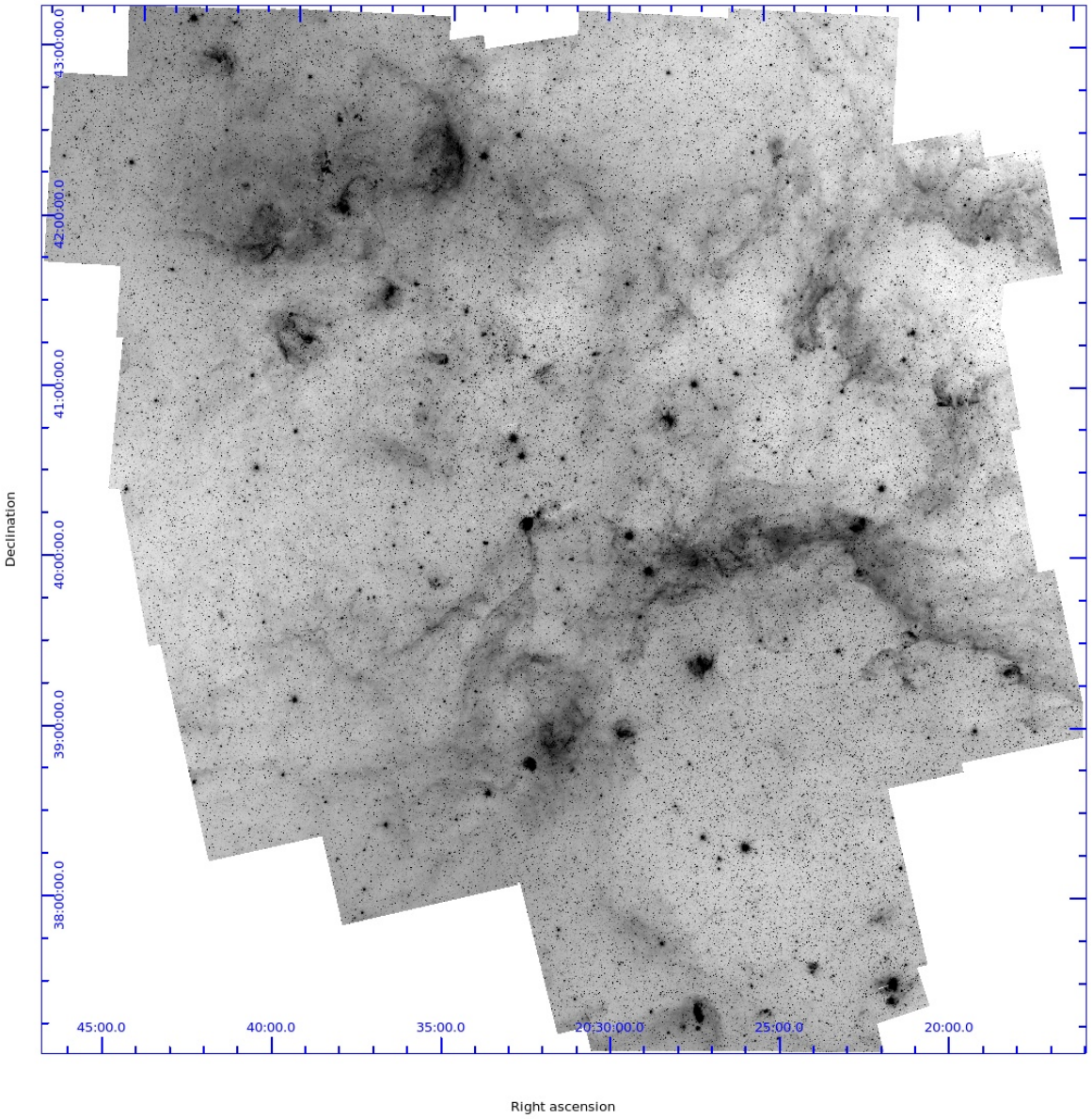

Figure 17. IRAC 4.5 μm full-field mosaic.

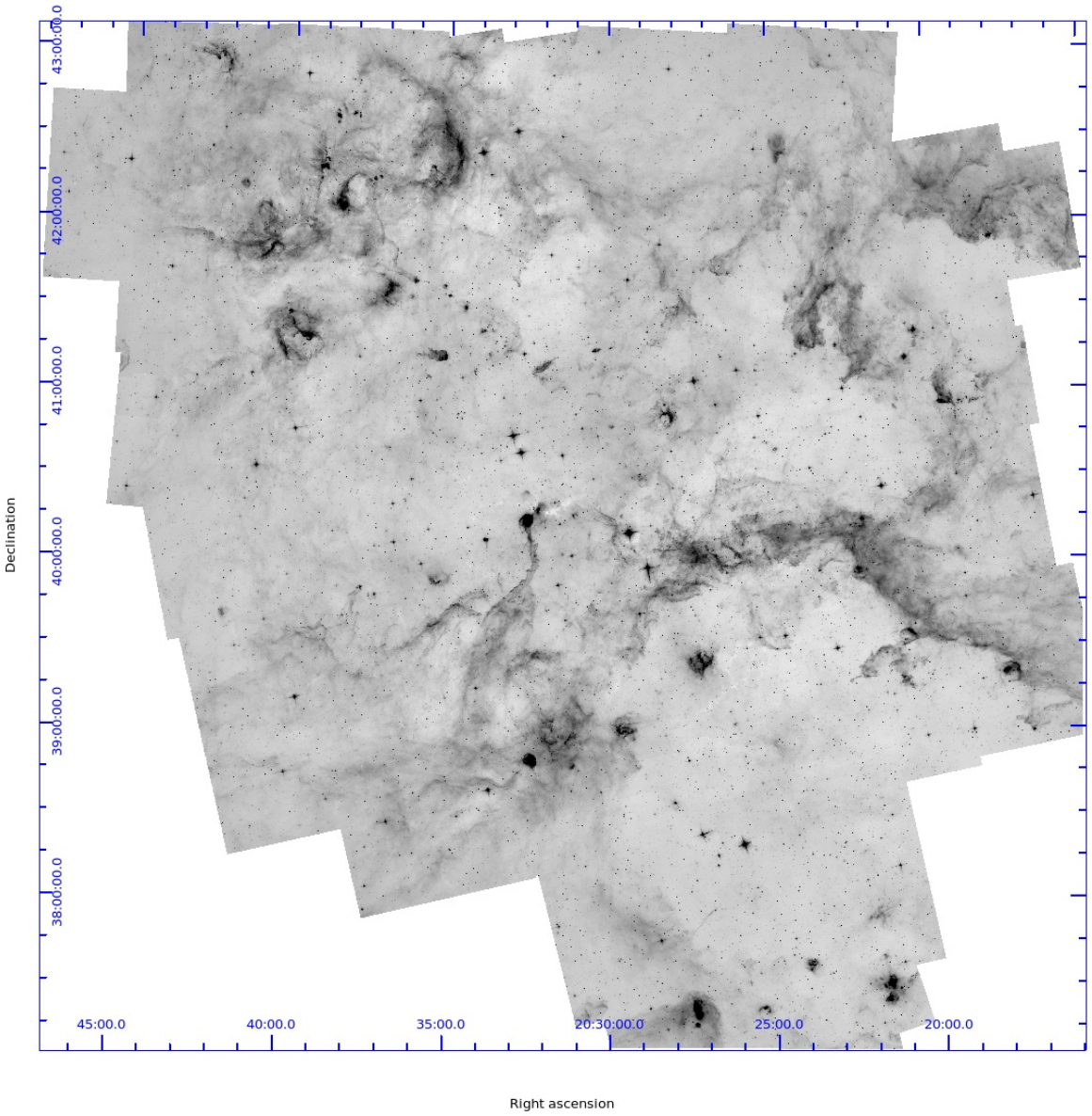

Figure 18. IRAC 5.8 μm full-field mosaic.

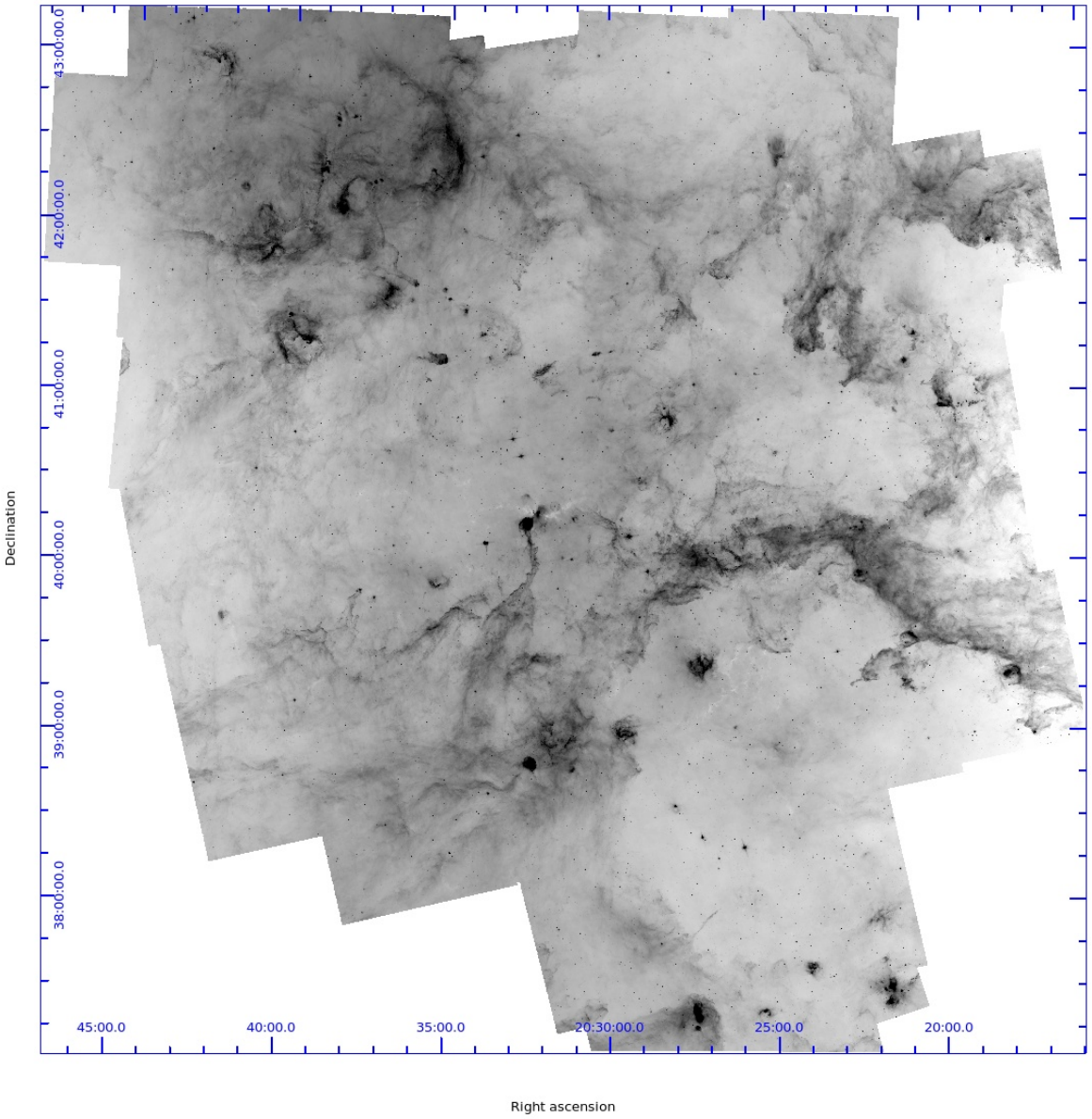

Figure 19. IRAC 8.0 μm full-field mosaic.

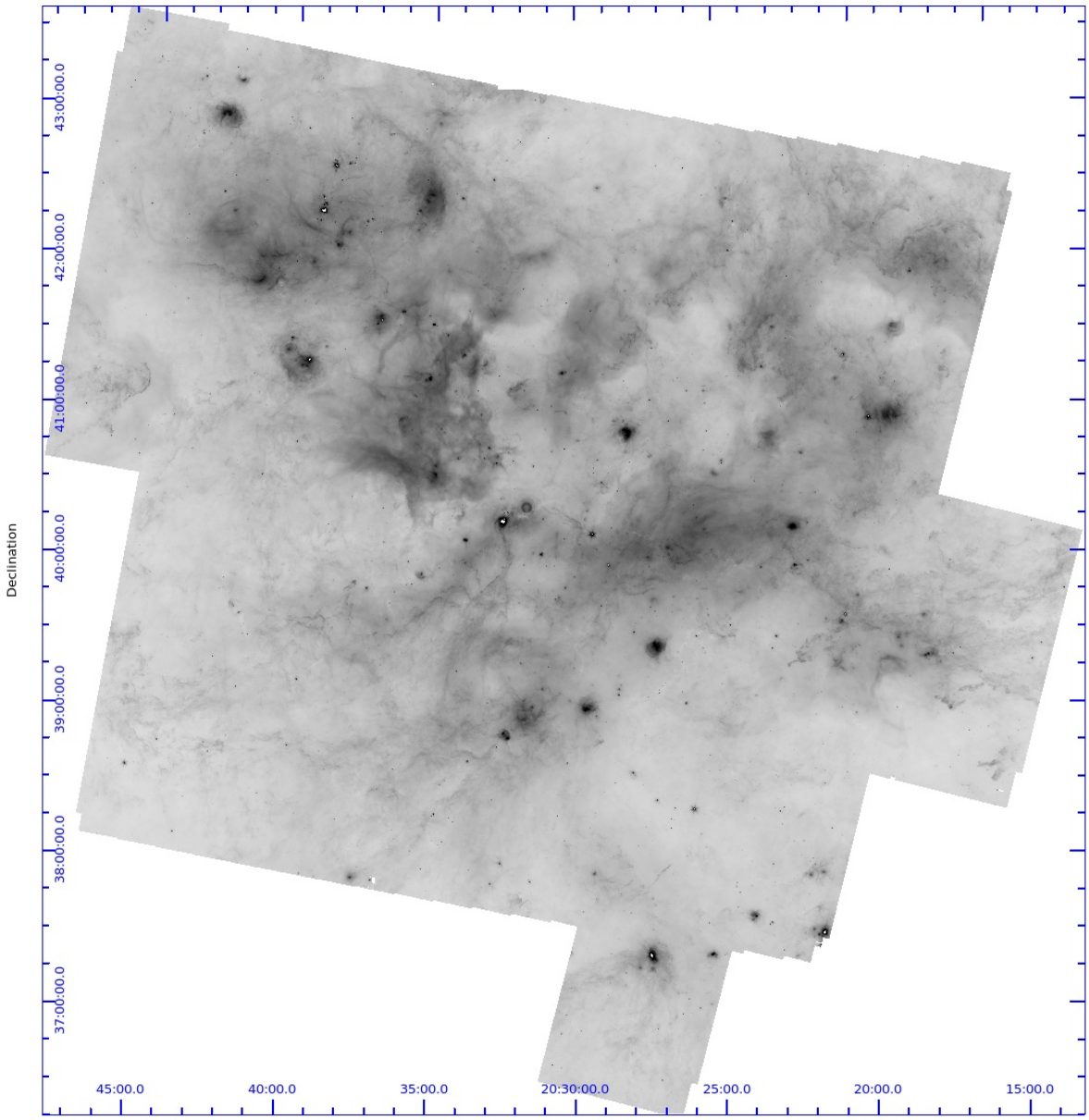

Figure 20. MIPS 24 μm mosaic.

3.2.3 Matching Tiles of the Full-Field Mosaics

Because the full-resolution images can be difficult to work with due to the memory requirements, we have divided the images into smaller overlapping tiles with the same RA and Decl. centers in order to be able to overlay them easily. These were produced by taking the highest resolution IRAC images (0.8626716 arcsec/pixel) and MIPS images (1.2 arcsec/pixel)

The IRAC mosaics have the file name of the form

Ix_cygnus_0.8_m_n.fits

where x is the channel number, and m and n are the row and column index of the image tile. All 0.8 images are subimages of the full Ix_cygnus_0.8.fits images listed above.

The MIPS mosaic tiles are subimages of the M1_cygnus_1.2.fits image above, and have the form

M1_cygnus_1.2_m_n.fits

where m and n are the row and column index values. The R.A. and Decl. positions for each of the tiles is given below in Table 4. Tiles with no valid pixels in the image are not included (e.g., tile 0_0 in all bands). An image of the tile layouts superimposed on the MIPS 24 μm image is shown in Figure 21.

Table 4. List of Tile Centers

	R.A.	Decl.
Tile	(J2000.0)	
1_0	309.117164	37.098746
2_0	307.239876	37.101560
3_0	305.364218	37.074810
0_1	311.056554	38.560601
1_1	309.141444	38.594821
2_1	307.223354	38.597798
3_1	305.307003	38.569500
4_1	303.396660	38.510136
0_2	311.124359	40.057687
1_2	309.166808	40.093820
2_2	307.206093	40.096964
3_2	305.247236	40.067083
4_2	303.294795	40.004404
0_3	311.195238	41.555278
1_3	309.193325	41.593360
2_3	307.188048	41.596674
3_3	305.184759	41.565181
4_3	303.188331	41.499124
0_4	311.269404	43.051323
1_4	309.221074	43.091390
2_4	307.169164	43.094877
3_4	305.119382	43.061742
4_4	303.076950	42.992247

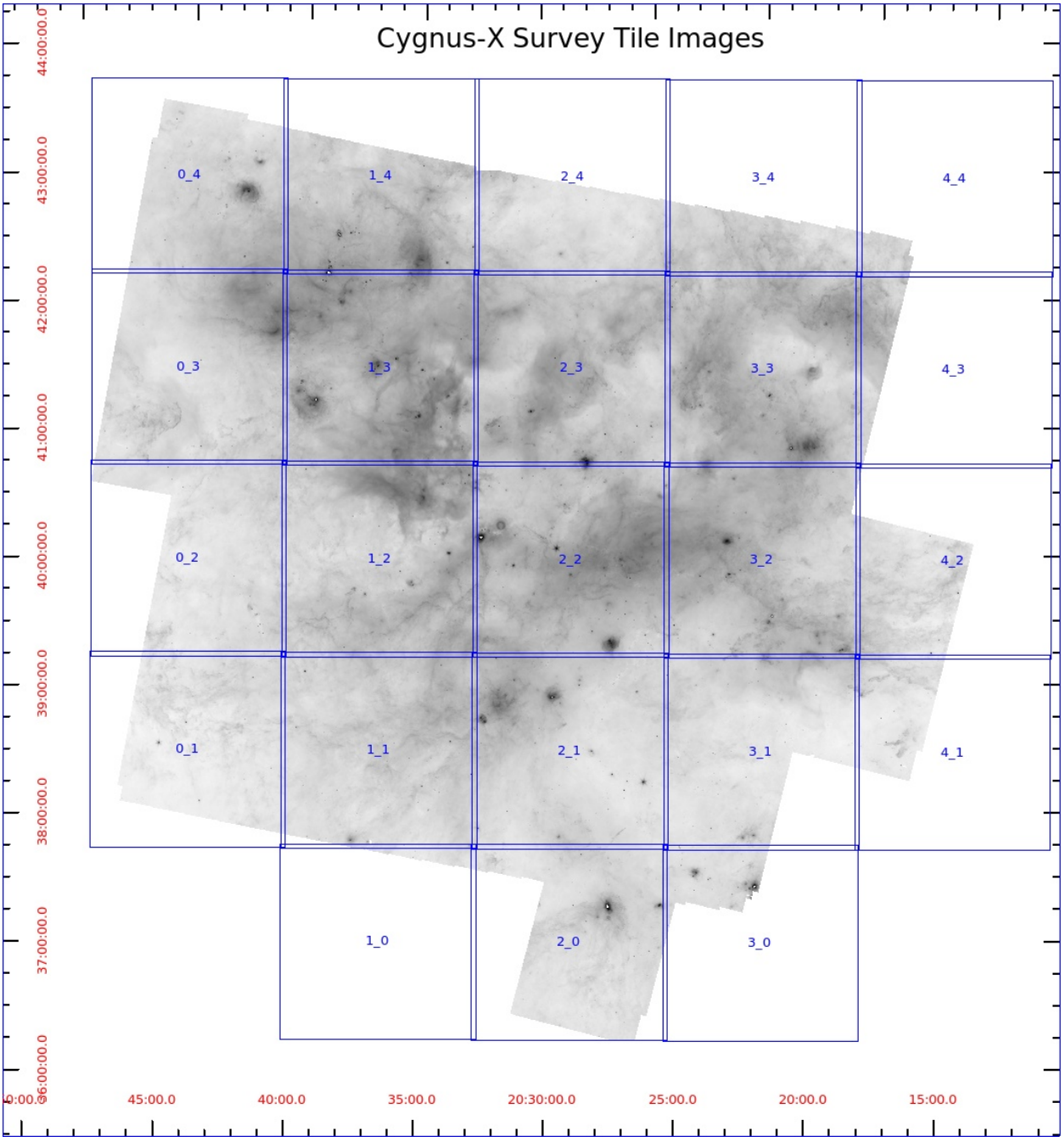

Figure 21. The MIPS 24μm image with image tiles overlayed. See Table 4 for a list of the tile center positions.

4. References

Beerer, I. M., Koenig, X. P., Hora, J. L., Gutermuth, R.A., Bontemps, S., Megeath, S. T., Schneider, N., Motte, F., Carey, S., Simon, R., Keto, E., Smith, H. A., Allen, L. E., Fazio, G. G., Kraemer, K. E., Price, S., Mizuno, D., Adams, J. D., Hernandez, J., Lucas, P. W. 2010, ApJ, 720, 679

Carey, S. J. et al. 2009, PASP, 121, 76

Gutermuth, R. et al. 2004, ApJS, 154, 374

Gutermuth, R. et al. 2008a, ApJ, 673, L151

Gutermuth, R. et al. 2008b, ApJ, 674, 336

Gutermuth, R., Megeath, S. T., Myers, P. C., Allen, L. E., Pipher, J. L., & Fazio, G. G. 2009, ApJS, 184, 18

Hora, J. L., Adams, J., Allen, L., Bontemps, S., Carey, S., Fazio, G., Gutermuth, R., Keto, E., Kraemer, K., Megeath, T., Mizuno, D., Motte, F., Price, S., Schneider, N., Simon, R., Smith, H. 2007, *A Spitzer Legacy Survey of the Cygnus-X Complex,* 2007sptz.prop40184H

Hora, J. L. et al. 2004, Proc. SPIE, 5487, 77

Hora, J. L. et al. 2008, PASP, 120, 1233F

Kraemer, K. E., Hora, J. L., Egan, M. P., Adams, J., Allen, L. E., Bontemps, S., Carey, S. J., Fazio, G. G., Gutermuth, R., Keto, E., Koenig, X. P., Megeath, S.T., Mizuno, D. R., Motte, F., Price, S. D., Schneider, N., Simon, R., Smith, H. 2010, AJ, 139, 2319

Makovoz, D., & Khan, I. 2005, in ASP Conf. Ser. 132, Astronomical Data Analysis Software and Systems VI, eds. P. L. Shopbell, M. C. Britton, & R. Ebert (San Francisco: ASP).

Megeath, S. T. et al. 2004, ApJS, 154, 367

Mizuno, D. et al. 2008, PASP, 120, 1028

Morales-Calderón, M. et al. 2011, ApJ, 733, 50

Pipher, J. L. et al. 2004, Proc. SPIE, 5487, 234

Reach, W. T. et al. 2005, PASP, 117, 978

Schneider, N., Bontemps, S., Simon, R., Jokob, H., Motte, F., Miller, M., & Kramer, C. 2006, A&A, 458, 855

Schneider, N., Simon, R., Bontemps, S., Comerón, F., & Motte, F. 2007, A&A, 474, 873

Schuster, M., Marengo, M., & Patten, B. 2006, SPIE, 6270, 74

Skrutskie, M. F. et al. 2006, AJ, 131, 1163

Stetson, P. B. 1987, PASP, 99, 191

5. Appendix – Data format

The catalogs are formatted in the IPAC table format. The first few lines of the files define the contents of each of the columns, and the actual data begins on the first line that does not contain a "|" character. The data are sorted in RA order, and then in Declination. Table 5 lists the data fields and their formats in the Archive and Catalog files. The table is in ASCII format with fixed column widths as defined in the header of the file. Where no valid data exists, the characters "null" appear in that column. The "Format" column gives the format specifier used in the print statement for the FLOAT or DOUBLE variable types when making the files. The "Width" column gives the width of the data column in ASCII spaces. All space not used by other characters is filled with the ASCII "space" character, no tabs are used.

The source fluxes were calculated from their magnitudes given in the other columns of the table. We used the zero magnitude fluxes in each channel as given by Reach et al. (2005) for IRAC (280.9, 179.7, 115.0, and 64.13 Jy for the 3.6, 4.5, 5.8, and 8.0 μm bands, respectively), and used 7.14 Jy for the MIPS 24 μm band based on the MIPS instrument handbook.

Table 5. Data format for Catalog and Archive datasets

Column Number	Name	Description	Units	Format	Width (chars)
1	ra	RA (J2000.0)	degree	10.6f	11
2	dec	Dec (J2000.0)	degree	10.6f	11
3	designation	Source designation of the form SSTCYGX JHHMMSS.SS+DDMMSS.S, where SST refers to the Spitzer Space Telescope, CYGX to the Cygnus-X Legacy Survey, HHMMSS.SS is the R.A. (J2000.0), DDMMSS.S is the Declination. Note that there is a space between the X and J in the name.		Char	28
4	2MASSJRA	2MASS J-band RA (J2000)	degree	10.6f	12
5	2MASSJDEC	2MASS J-band Dec (J2000)	degree	10.6f	11
6	2MASSHRA	2MASS H-band RA (J2000)	degree	10.6f	12
7	2MASSHDEC	2MASS H-band Dec (J2000)	degree	10.6f	11
8	2MASSKRA	2MASS K-band RA (J2000)	degree	10.6f	12
9	2MASSKDEC	2MASS K-band Dec (J2000)	degree	10.6f	11
10	IRACI1RA	IRAC Channel 1 RA (J2000)	degree	10.6f	12
11	IRACI1DEC	IRAC Channel 1 Dec (J2000)	degree	10.6f	11
12	IRACI2RA	IRAC Channel 2 RA (J2000)	degree	10.6f	12
13	IRACI2DEC	IRAC Channel 2 Dec (J2000)	degree	10.6f	11
14	IRACI3RA	IRAC Channel 3 RA (J2000)	degree	10.6f	12
15	IRACI3DEC	IRAC Channel 3 Dec (J2000)	degree	10.6f	11
16	IRACI4RA	IRAC Channel 4 RA (J2000)	degree	10.6f	12
17	IRACI4DEC	IRAC Channel 4 Dec (J2000)	degree	10.6f	11
18	Jmag	2MASS J-band magnitude	mag	8.3f	9

19	Hmag	2MASS H-band magnitude	mag	8.3f	9
20	Kmag	2MASS K-band magnitude	mag	8.3f	9
21	I1mag	IRAC Channel 1 magnitude	mag	8.3f	9
22	I2mag	IRAC Channel 2 magnitude	mag	8.3f	9
23	I3mag	IRAC Channel 3 magnitude	mag	8.3f	9
24	I4mag	IRAC Channel 4 magnitude	mag	8.3f	9
25	eJmag	2MASS J-band magnitude uncertainty	mag	6.3f	7
26	eHmag	2MASS H-band magnitude uncertainty	mag	6.3f	7
27	eKmag	2MASS K-band magnitude uncertainty	mag	6.3f	7
28	I1mage	IRAC Channel 1 magnitude uncertainty	mag	6.3f	8
29	I2mage	IRAC Channel 2 magnitude uncertainty	mag	6.3f	8
30	I3mage	IRAC Channel 3 magnitude uncertainty	mag	6.3f	8
31	I4mage	IRAC Channel 4 magnitude uncertainty	mag	6.3f	8
32	MIPSRA	MIPS 24micron source RA (J2000)	degree	10.6f	11
33	MIPSDEC	MIPS 24micron source Dec (J2000)	degree	10.6f	11
34	M24mag	MIPS 24micron magnitude	mag	8.3f	9
35	M24merr	MIPS 24micron magnitude uncertainty	mag	8.3f	9
36	M24_FWHM	MIPS 24micron source Full width half maximum diameter	arcsec	8.4f	9
37	M24_d	Distance between MIPS and IRAC source position	arcsec	8.3f	9
38	I1flux	IRAC Channel 1 Flux Density	uJy	11.1f	13
39	I2flux	IRAC Channel 2 Flux Density	uJy	11.1f	13
40	I3flux	IRAC Channel 3 Flux Density	uJy	11.1f	13
41	I4flux	IRAC Channel 4 Flux Density	uJy	11.1f	13
42	M24flux	MIPS 24micron Flux Density	uJy	11.1f	13
43	I1ferr	IRAC Channel 1 Flux Density uncertainty	uJy	9.1f	11
44	I2ferr	IRAC Channel 2 Flux Density uncertainty	uJy	9.1f	11
45	I3ferr	IRAC Channel 3 Flux Density uncertainty	uJy	9.1f	11
46	I4ferr	IRAC Channel 4 Flux Density uncertainty	uJy	9.1f	11
47	M24ferr	MIPS 24micron Flux Density uncertainty	uJy	9.1f	11